Fifth Annual NASA Workshop on Fluids and Heat Transfer Analysis
NASA Lewis Research Center-Ohio Aerospace Institute, Cleveland, OH, Aug.16-20, 1993
NASA CP 10122, pp. 467-476.

UNSTEADY THREE-DIMENSIONAL THERMAL FIELD PREDICTION IN TURBINE BLADES USING NONLINEAR BEM

Thomas J. Martin* and George S. Dulikravich*
Department of Aerospace Engineering
The Pennsylvania State University, University Park, PA 16802, USA

SUMMARY

A time-and-space accurate and computationally efficient fully three-dimensional unsteady temperature field analysis computer code has been developed for truly arbitrary configurations. It uses Boundary Element Method (BEM) formulation based on an unsteady Green's function approach, multi-point Gaussian quadrature spatial integration on each panel, and a highly clustered time-step integration. The code accepts either temperatures or heat fluxes as boundary conditions that can vary in time on a point-by-point basis. Comparisons of the BEM numerical results and known analytical unsteady results for simple shapes demonstrate very high accuracy and reliability of the algorithm. An example of computed three-dimensional temperature and heat flux fields in a realistically shaped internally cooled turbine blade is also discussed.

INTRODUCTION

For linear boundary-value and initial-value problems it is computationally more efficient to use BEM rather than finite differencing or finite element technique. An additional benefit is that the BEM requires a relatively coarse grid and that it can be easily extended to non-linear conduction problems via Kirchoff's transformation. Probably the most important fact is that the BEM is essentially a non-iterative technique thus making the BEM codes more reliable [Dulikravich and Hayes 1988; Dargush and Banerjee 1991].

THEORY OF 3-D BOUNDARY ELEMENTS

The governing equation for heat conduction in the absence of heat generators is

$$\frac{\partial u}{\partial t} = \alpha \nabla^2 u \tag{1}$$

where α is the thermal diffusivity such that $\alpha = k/\rho c$, k is the thermal conductivity, ρ is the mass density, and c is the specific heat. As the problem is now time-dependent, the weighted residual statement must be integrated with relation to time and space. After integration by parts twice [Brebbia and Dominguez 1989], one obtains

$$\int_{t_0}^{t}\int_{\Omega}\left(\nabla^2 u^* - \frac{1}{\alpha}\frac{\partial u^*}{\partial t}\right) u \, d\Omega \, d\tau + \int_{t_0}^{t}\int_{\Gamma} q\, u^* \, d\Gamma \, d\tau = \int_{t_0}^{t}\int_{\Gamma} u\, q^* \, d\Gamma \, d\tau + \left[\int_{\Omega} u\, u^* \, d\Omega\right]_{\tau=t_0}^{\tau=t} \tag{2}$$

where $t_0 < \tau < t$ and the $\partial u^*/\partial t$ term was obtained integrating by parts with respect to time.

---

* Graduate Research Assistant.

* Associate Profesor.

The corresponding fundamental solution for this equation is

$$u^* = \frac{1}{[4\pi\alpha(t-\tau)]^{D/2}} \exp\left[\frac{-r^2}{4\alpha(t-\tau)}\right] \tag{3}$$

where D is the number of spatial dimensionality, that is, D = 3 for three-dimensional problems and r is the distance from the point of integration, x_j, to the observation point, x_i. The fundamental solution satisfies the auxiliary equation

$$\nabla^2 u^* - \frac{1}{\alpha}\frac{\partial u^*}{\partial t} = 0 \tag{4}$$

and for $t = \tau$,

$$\int_\Omega u^* \, d\Omega = \begin{cases} 0 \text{ for } r \neq 0 \\ 1 \text{ for } r = 0 \end{cases} \tag{5}$$

Using these relations, one obtains the boundary element equation for the ith control point

$$c_i u_i + \int_{t_0}^{t}\int_\Gamma u\, q^* \, d\Gamma \, d\tau = \int_{t_0}^{t}\int_\Gamma q\, u^* \, d\Gamma \, d\tau + \left[\int_\Omega u\, u^* \, d\Omega\right]_{\tau=t_0} \tag{6}$$

The last term in the above formula represents the contribution of the initial state at $t = t_0$. Since the fundamental solution is time dependent, one does not need to solve this equation with an iterative scheme as is usually done in finite elements or finite differences. Instead, this equation can be solved for any time step after a known initial state although small time intervals are recommended. In the latter case, the potential at each node within the domain needs to be evaluated at the end of each time step in order to determine the initial conditions for the next time step. Although the primary advantage of boundary elements is lost (for unsteady problems, the discretization of the volume is necessary), the matrix is much smaller than those in finite elements and the inversion needs only be performed once if time-independent boundary conditions are enforced.

The region, Ω, and bounding surface, Γ, are discretized into N_{CELL} volume cells utilizing a total of N_{TOT} nodes and N_{SP} surface elements using a total N nodes. Nodal quantities are interpolated linearly across each individual cell or surface panel. One also needs to assume a variation in time for the functions u and q. If these functions do not vary significantly with respect to time, they may be treated as constant over small time intervals and the time integration may be performed stepwise. If greater accuracy is required, these functions may be assumed to vary linearly such that

$$u(x_i, x_j, t, \tau) = \frac{\tau - t_0}{\Delta t} u + \frac{t - \tau}{\Delta t} u_0 \tag{7}$$

where the subscript 0 indicate the variable at the previous time level and t is the current time level. The time step is defined as $\Delta t = t - t_0$. Once fully discretized, the boundary element equation may be expressed as

$$[H]\,U = [G]\,Q + P \tag{8}$$

for constant time elements. If linearly varying time elements are used, the boundary element

equation becomes

$$[\mathbf{H}]\,\mathbf{U} + [\mathbf{H}_0]\,\mathbf{U}_0 = [\mathbf{G}]\,\mathbf{Q} + [\mathbf{G}_0]\,\mathbf{Q}_0 + \mathbf{P} \tag{9}$$

The term $\mathbf{U} = (u_1, u_2, u_3, \ldots, u_N)$ is the vector of potentials and $\mathbf{Q} = (q_1, q_2, q_3, \ldots, q_{Nsp})$ is a vector of fluxes where each term q_i contains four potential derivatives corresponding to the corner vertices of the N_{SP} quadrilateral surface panels. In addition, each term in the [G] matrix contains four terms corresponding to each q_i term. The terms in the [H] matrix are the properly summed coefficients corresponding to the potential at a specific node. The boundary element algorithm developed for use in three-dimensions with the inverse design code was formulated with isoparametric, quadrilateral surface panels and eight-point linearly deformed parallelepiped volume cells. Integration in space was done numerically with Gaussian quadrature and time integration was performed numerically using the trapezoid rule. Since the fundamental solutions contain a singularity at the end of each time step (at the time level $\tau = t$), the time integration points were clustered strongly near the singularity, $\tau = t$.

A transformation from the global (ξ,η,ζ) coordinate system is necessary to a localized (ξ_1,ξ_2) coordinate system defined over the surface of the body or to a (ξ,η,ζ) coordinate system defined for the volume cell of integration. The volume integrals are transformed such that

$$\int_{\Omega} u\, u^*\, d\Omega = \iiint u\, u^*\, |J|\, d\xi\, d\eta\, d\zeta \tag{10}$$

where $|J|$ is the determinant of the Jacobian matrix of the transformation, that is,

$$|J| = \det\left(\frac{\partial(x,y,z)}{\partial(\xi,\eta,\zeta)}\right). \tag{11}$$

The terms of the **G** and **H** matrices for constant time elements may be written as

$$\mathbf{H}_{im} = \sum_{k=1}^{N_c} \int_{t_0}^{t} \int_{\Gamma_j} \phi_k\, q^*\, d\Gamma_j\, d\tau \quad \text{and} \quad \mathbf{G}_{ijk} = \int_{t_0}^{t} \int_{\Gamma_j} \phi_k\, u^*\, d\Gamma_j\, d\tau \tag{12}$$

for the jth surface panel. The subscript m indicates the node number corresponding to the kth vertex of the jth surface panel and N_C is the number of surface panels connected to the mth node. The function f_k is the kth interpolation function corresponding to the value at the kth corner vertex of the jth surface panel. Discretization of the surface is identical to that described in section 2.2. If linearly varying time elements are used, the terms of the [G] and [H] matrices are similar and are formed into pairs of coefficient matrices due to the initial state and the current time level at the boundary.

$$\mathbf{H}_{im0} = \sum_{k=1}^{N_c} \int_{t_0}^{t} \int_{\Gamma_j} \phi_k \frac{\tau - t_0}{\Delta t}\, q^*\, d\Gamma_j\, d\tau \tag{13}$$

$$\mathbf{H}_{im} = \sum_{k=1}^{N_c} \int_{t_0}^{t} \int_{\Gamma_j} \phi_k \frac{t - \tau}{\Delta t} q^* \, d\Gamma_j \, d\tau \tag{14}$$

The vector **P** indicates the contribution of the initial state throughout the domain on the ith observation point and is of the form

$$\mathbf{P}_i = \sum_{j=1}^{N_{CELL}} \sum_{k=1}^{8} u_{0jk} \int_{\Omega_j} \phi_k \, u^* \, d\Omega_j \tag{15}$$

where ϕ_k is the kth trilinear interpolation function of the linearly deformed parallelepiped cell and is of the form

$$\phi_k = \frac{1}{8}(1 \pm \xi)(1 \pm \eta)(1 \pm \zeta) \tag{16}$$

The term u_{0jk} is the potential on the kth vertex of the jth parallelepiped volume cell at time $\tau = t_0$. In discretized form, the fundamental solution contains the term r representing the distance from the point of integration on the jth volume cell or surface panel to the ith control point. The normal derivative of the fundamental solution may be determined as

$$q^* = \frac{\partial u^*}{\partial r} \frac{\partial r}{\partial n} = \frac{-d}{[4\pi\alpha(t - \tau)]^{D/2} 2\alpha(t - \tau)} \exp\left[\frac{-r^2}{4\alpha(t - \tau)}\right] \tag{17}$$

where d is defined by the normal distance from the ith point under consideration to the surface panel. If the control point is on the surface of integration, then $q^* = 0$ and the diagonal of [**H**] may be computed implicitly by the application of a uniform potential over the whole domain, which will give zero normal fluxes at the boundaries such that

$$\mathbf{H}_{ii} = - \sum_{j=1}^{N_N} \mathbf{H}_{ij} + \mathbf{P}_i \tag{18}$$

NUMERICAL RESULTS

The accuracy and reliability of the BEM formulation governing three-dimensional, unsteady heat transfer problems has been verified versus the analytical solution for a finite length rod. Total surface of a cylinder of 0.5 m radius and 1.0 m in length was modeled with 216 nodes and 108 surface panels as shown in Figure 1. The thermal diffusivity, α, was specified to be 1.0 $m^2 s^{-1}$. The initial temperature of the cylinder was uniformly 0 °C and contained no heat sources or sinks. Then, suddenly, the boundary conditions on the cylinder were specified as 100 °C on the front face, 0 °C on the back face while the outer radial surface was kept adiabatic. The BEM algorithm used constant time interpolation, 3-point Gaussian quadrature for the surface and volume integration and a linear variation of the temperature and heat flux along the surface panels and volume cells. The analytic solution for this test case corresponded to the one-dimensional unsteady heat flow in a finite thin rod. Temperatures were obtained at various time levels and at several axial locations and are compared to the analytic results shown in Figure 2. As seen in this figure, there is a discrepancy between the numerical and analytic solutions averaging about 6 °C.

The geometry of the cylinder was then modeled differently by slightly clustering the surface panels and volume cells near the hot end. Figure 3 shows the results of the BEM in this case.

Notice that the average error has reduced to about 4 °C. The unsteady BEM algorithm was then developed with a linear variation within each time step for the temperatures and heat fluxes. This test case used the same slightly clustered geometry with identical boundary and initial conditions. A single BEM analysis run using linear time interpolation consumed about 15% more CPU time than the BEM formulation with constant time interpolation. It resulted in a solution which averaged a 3 °C error compared to the analytic solution. Figure 4 shows the computed temperatures from the BEM using linear time interpolation against the analytic solution at several axial locations. Figure 5 is a plot of the error between the BEM and the analytic solution.

The accuracy of the BEM algorithm could not be improved further while using the cylinder test case. Instead, a different and simpler geometry was developed and the BEM solution with this new geometry showed that much of the error in the previous tests was due to the cylindrical geometry. That is, since the BEM uses flat quadrilateral surface panels, the exact geometry of the cylinder surface could not be modeled properly. Figure 1 shows a discretized cross section of the circular cylinder and clearly depicts the inability of a limited number of flat surface panels to properly capture the surface curvature of the cylinder. Besides, elements surrounding the cylinder axis are nearly triangular in shape. These situations produce surface and volume integrals which behave somewhat singularly. The result is that the integrals are not properly integrated and may involve ill-conditioned BEM solution matrices.

The new geometry, a rectangular box of 0.1 m x 0.1 m base cross section and 1.0 m in length, was then used instead of the cylinder. The geometry was divided into 10 axial cells of equal size. The entire surface of the box was discretized with 44 nodes (four nodes per each section) and 44 flat quadrilateral surface panels (four side panels per each section). The boundary conditions on the box were specified as 100 °C on the front face, 0 °C on the back face while the side surfaces were kept adiabatic. The BEM algorithm used linear time interpolation, 5-point Gaussian quadrature and a linear variation of the temperature and heat flux along the surface panels and volume cells. Temperatures obtained with the unsteady BEM algorithm for the rectangular box were compared to the analytic solution at several axial locations. Figure 6 illustrates that the BEM solution for the box was much more accurate than those for the cylinder. Figure 7 shows the absolute value of the error in the temperatures computed using the BEM. These results indicate that the BEM generates an error of 0.5 °C with the maximum error below 0.9 °C.

The unsteady BEM algorithm was then modified to incorporate temperature-dependent material properties. Although the BEM solution of the linear heat conduction equation is quite fast (requiring less than 10 CPU seconds for 25 time steps on an IBM 3090 for the rectangular box), the addition of temperature-dependent material properties greatly increases the computational effort. Normally the BEM solution matrices need only to be computed once if the time intervals and diffusivity are constant. Since the diffusivity is now a function of temperature, the BEM solution matrices need to be developed at each time interval using temperatures computed at each source point in the surface and volume integrands.

The same rectangular box geometry and boundary conditions were used to test the accuracy of the three-dimensional, unsteady BEM algorithm with temperature-dependent material properties. The reference thermal conductivity was $\lambda_o = 1.0$ kcal m^{-1} s^{-1} K^{-1} and it varied linearly with temperature as $\lambda = \lambda_o + C\,T$. The temperature variations in time at a single axial location were collected for various degrees of nonlinearity given by the parameter C. These results are shown in Figure 8 and compare well with published computational results involving finite elements [Tanaka, Kikuta and Togoh 1987]. Total CPU time for 25 time steps with the temperature-dependent physical properties was approximately 300 seconds on an IBM 3090.

CONCLUSIONS

A fully three-dimensional unsteady heat conduction analysis code has been successfully developed and tested against known analytical solutions. The code is computationally efficient and reliable and can be used on arbitrary configurations. A modification involving temperature-dependent thermal diffusivity was also incorporated and shown to produce good results.

REFERENCES

Brebbia, C.A. and Dominguez, J.: Boundary Elements: An Introductory Course. McGraw-Hill Book Company, 1989.

Dargush, G.F. and Banerjee, P.K.: Application of the Boundary Element Method to Transient Heat Conduction. International Journal for Numerical Methods in Engineering, Vol. 31, 1991, pp. 1231-1247.

Dulikravich, G.S. and Hayes, L.J.; Control of Surface Temperatures to Optimize Survival in Cryopreservation, ASME Winter Annual Meeting", Proceedings of the Symposium on Computational Methods in Bioengineering, Editors: R.L. Spilker and B.R. Simon, Nov. 27-Dec. 2, 1988, ASME BED-Vol. 9, 1988, pp. 255-265.

Tanaka, M., Kikuta, M. and Togoh, H.: Boundary Element Analysis of Nonlinear Transient Heat Conduction Problems. Computer Methods in Applied Mechanics and Engineering, Vol. 62, No. 3, June 1987, pp. 321-329.

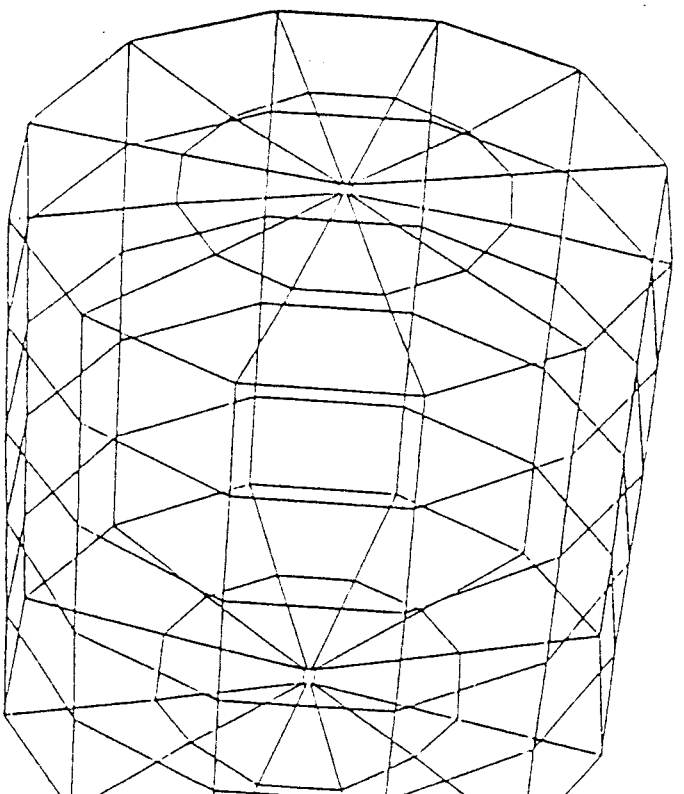

Figure 1. Geometry of a cylinder for the verification of the three-dimensional, unsteady BEM formulation.

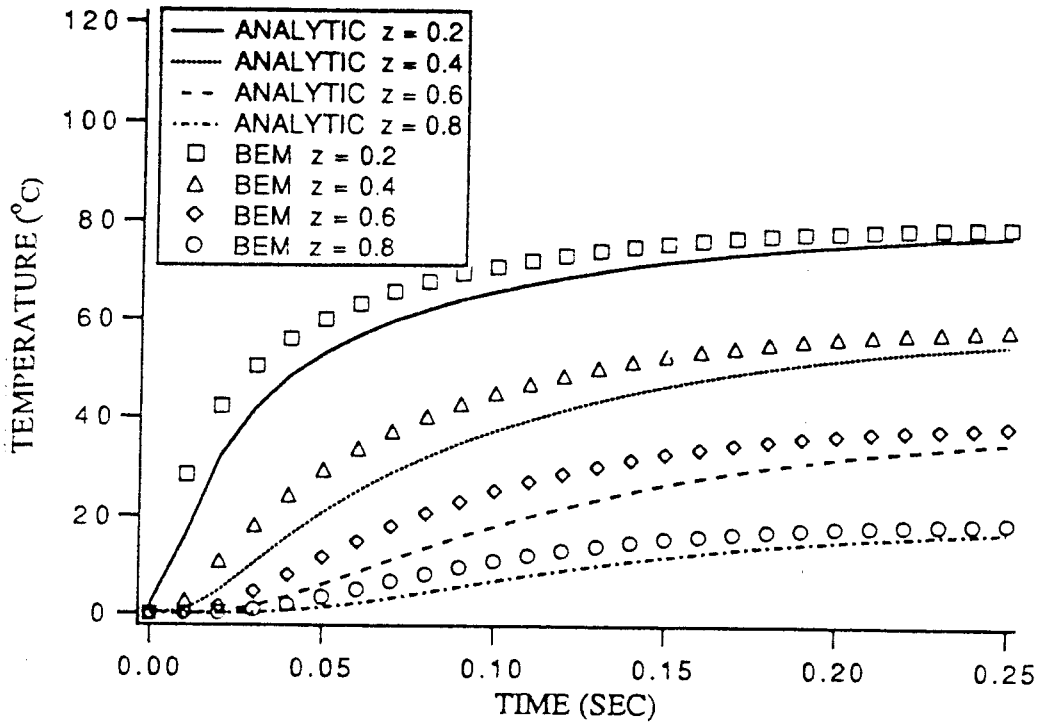

Figure 2. Comparison of temperatures between the unsteady BEM solution and the analytic solution using constant time elements.

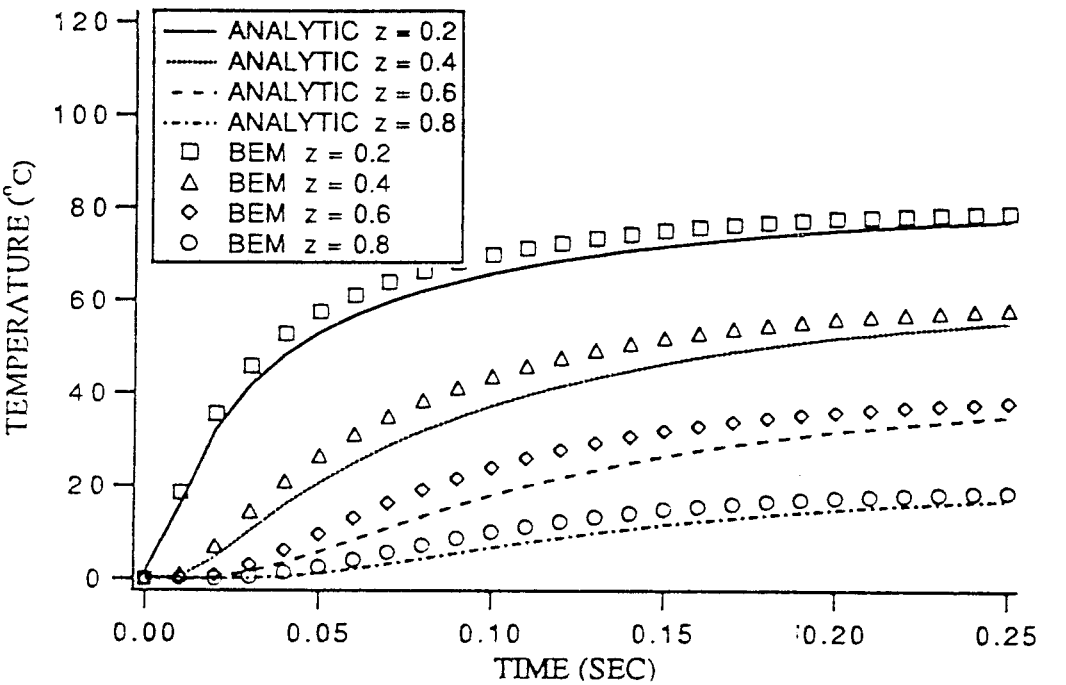

Figure 3. Comparison of temperatures between the unsteady BEM solution and the analytic solution using a refined grid and constant time elements.

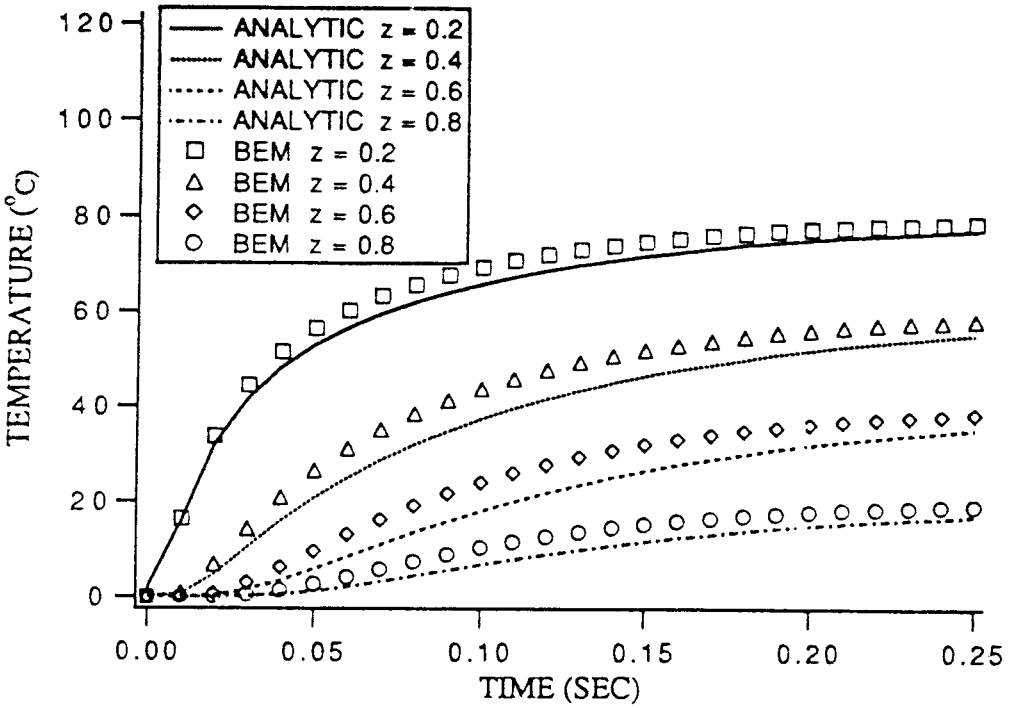

Figure 4. Comparison of temperatures between the unsteady BEM solution and the analytic solution using a refined grid and linear time elements.

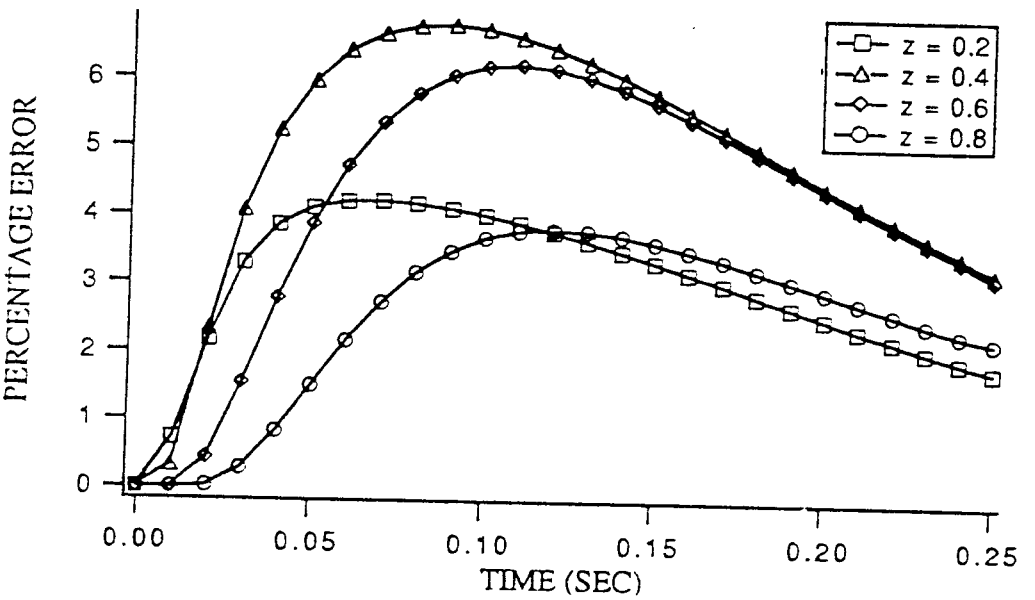

Figure 5. Relative error in temperature between the unsteady BEM solution and the analytic solution using a refined grid and linear time elements.

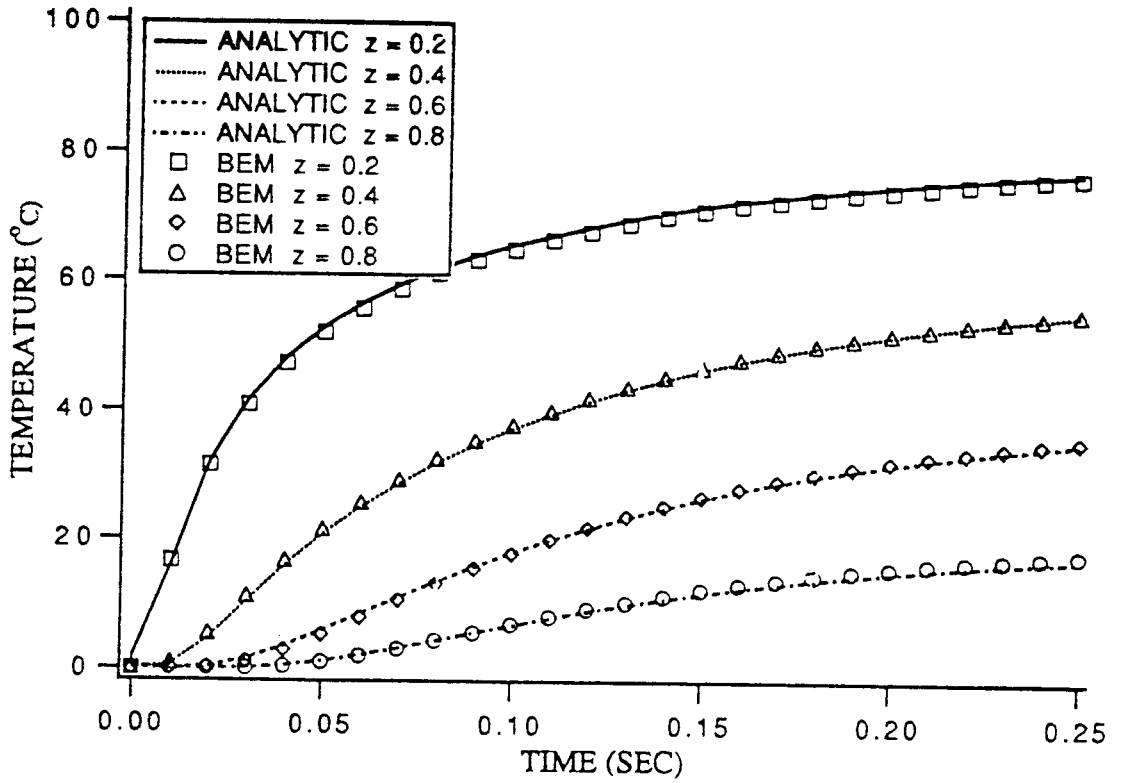

Figure 6. Comparison of temperatures between the unsteady BEM solution of a rectangular box and the analytic solution using linear time interpolation and accurate quadrature integration.

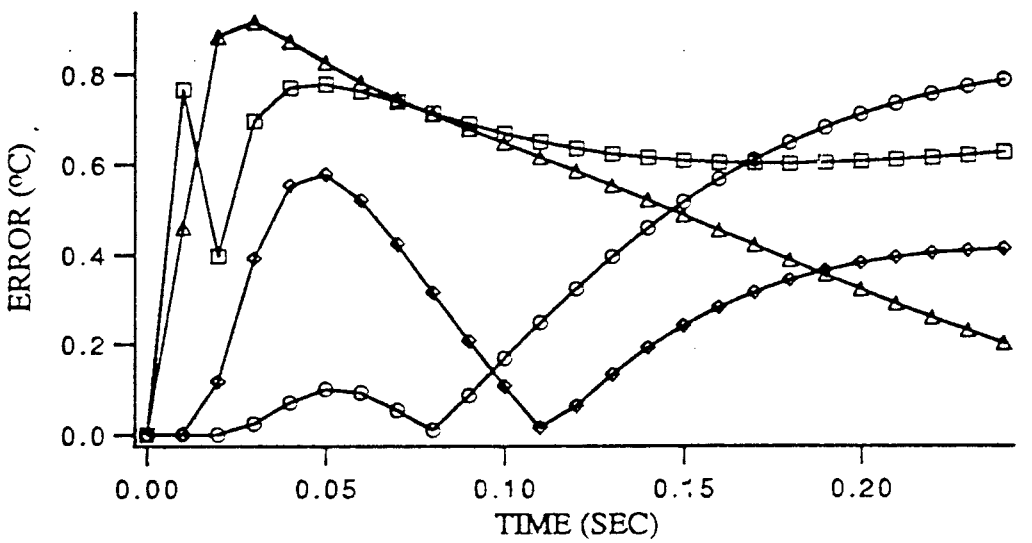

Figure 7 . Error in temperature between the unsteady BEM solution of a rectangular box and the analytic solution.

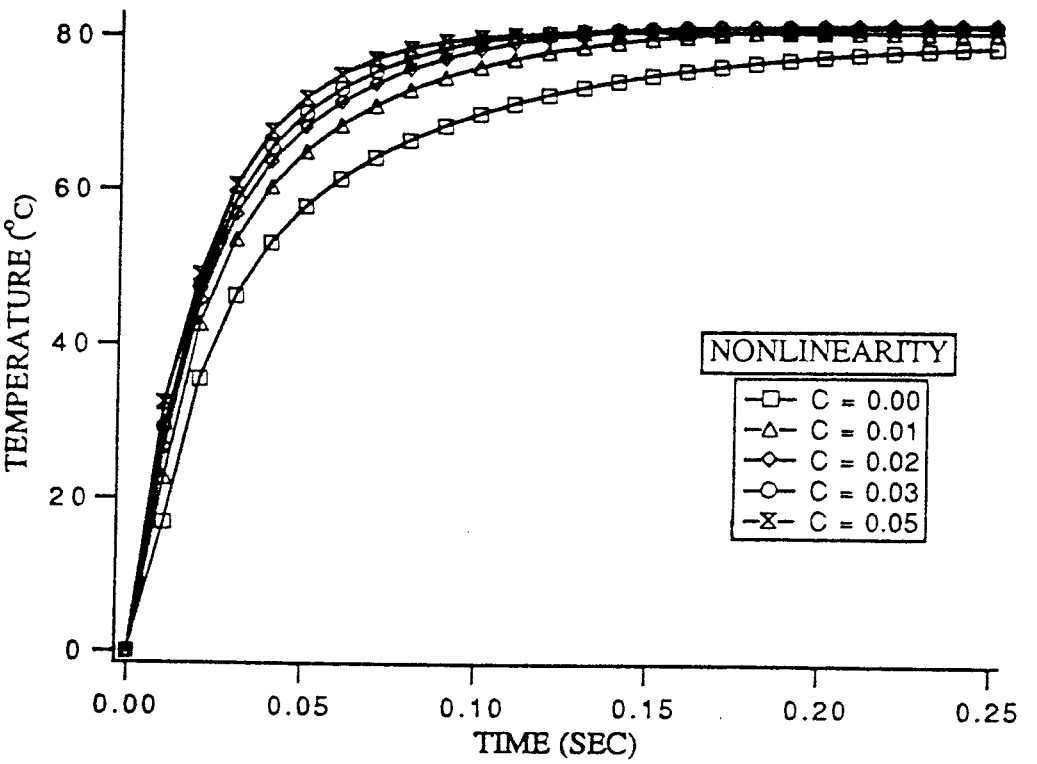

Figure 8 Results of the unsteady BEM algorithm with temperature-dependent material properties. The figure shows temperatures versus time at the z = 0.2 m axial location for various ranges of nonlinearity.